Enzymatic Cross-Linking versus Radical Polymerization in the Preparation of Gelatin PolyHIPEs and Their Performance as Scaffolds in the Culture of Hepatocytes

Andrea Barbetta,*,† Mara Massimi,*,‡ Laura Conti Devirgiliis,‡ and Mariella Dentini†

Department of Chemistry, University of Rome "La Sapienza", P.le A. Moro 5, 00185 Rome, Italy, and Department of Basic and Applied Biology, University of L'Aquila, via Vetoio, 67010 L'Aquila, Italy

Received June 5, 2006; Revised Manuscript Received July 31, 2006

Highly open porous biodegradable scaffolds, based on gelatin A3, were fabricated with the aim of using them for tissue-engineering applications. The fabrication process is based on an emulsion-templating technique. In the preparation of gelatin scaffolds two different cross-linking procedures were adopted: (I) radical polymerization of the methacrylate functionalities, previously introduced onto the gelatin chains and (II) formation of isopeptide bridges among the gelatin chains promoted by the enzyme microbial transglutaminase. The method of cross-linking exerts a pronounced effect on the morphology of the porous biomaterials: radical polymerization of methacrylated gelatin allowed the production of scaffolds with a better defined porous structure, while the enzymatically cross-linked scaffolds were characterized by a thinner skeletal framework. A suitable sample of each kind of the differently cross-linked porous biomaterials was tested for the culture of hepatocytes. The scaffold obtained by radical polymerization possessed a morphology characterized by relatively large voids and interconnects, and as a consequence, it was more suitable for hepatocytes colonization. On the other hand, the enzymatically cross-linked scaffold resulted in less cytotoxicity and the cultured hepatocytes expressed a better differentiated phenotype, as evidenced by a greater expression and more correct localization of key adhesion proteins.

1. Introduction

Hydrogels are materials becoming increasingly important in many biomedical applications such as skin substitutes, adhesives, matrixes for drug delivery, and scaffolds for tissue engineering.

State of the art experience dictates that parameters determining hydrogel scaffold performance should be the chemical chain composition, the nature of the "junction zones" (physical gels) or of the bridging units (chemical gels), the capacity to interact and hold water molecules, and last but not least, the porosity. Cell scaffolds must in fact ensure favorable cell−chains contacts, diffusion of cells and nutrients inside (metabolites outside) the network, possible cells clustering if required (as in the case of hepatocytes) so that biological performance of the whole system may be satisfactory and long lasting.

As part of our ongoing research project focused on the production of novel scaffolds that mimic the in vivo cellular microenvironment, we used naturally occurring biopolymers as components of the scaffolds together with a high internal phase emulsion (HIPE) polymerization route as the fabrication process. This method allows the synthesis of solid foams characterized by a highly porous and fully interconnected morphology. So far, different kinds of polymers have been used as building components of the solid foams: poly(styrene-*co*-divinylbenzene),[1−3] poly(caprolactone-*co*-styrene),[4] poly(lactic acid-*co*-styrene),[5] and more recently dextran, pullulan, and gelatin.[6,7]

The last-mentioned biopolymers have a well-established record of applications in the biomedical field,[8] and the derived scaffolds are expected to show biocompatibility towards the seeded cells.

However, in the approach we have previously developed, these biomacromolecules were subjected to chemical derivatization with methacrylate groups in order to be able to undergo cross-linking by radical polymerization and to meet the demands of long-term clinical use.

It is recently becoming more recognized that the context in which cells are grown is fundamental, and by changing their environment, cells can radically alter their behavior. We wondered whether a cross-linking method which avoids the introduction of foreign chemical functionalities on the biopolymeric chains might contribute in improving the biocompatibility of the scaffolds. In this respect, an enzymatic cross-linking process will be of obvious advantage because it would allow the production of porous chemical gels endowed with at least the same biocompatibility as the starting biopolymers.[9] Therefore, the goal of this work was to prepare gelatin A3 polyHIPE scaffolds using two different cross-linking procedures: a "conventional" one,[6,7] involving radical polymerization of the methacrylated derivative of gelatin, and a novel one, involving the formation of isopeptide bonds between the γ-carbonyl group of a glutamine residue and the ϵ-amino group of a lysine residue catalyzed by microbial transglutaminase (MTGase).[10] This enzyme has been used mainly in the food industry, but recently it has found application in the biomedical field as an in situ self-cross-linking agent forming biodegradable gelatin[11] or mixed gelatin−chitosan,[12] fibrin,[13] and collagen[14] scaffolds. To our knowledge, this is the first time that MTGase was employed in the preparation of porous biomaterials using the HIPE methodology.

The two differently cross-linked types of gelatin-based biomaterials were morphologically characterized, and their performances as scaffolds in the culture of hepatocytes were

* Corresponding authors. Phone: +39-06-49913633 (A.B.); +39-0862-433290 (M.M.). Fax: +39-06-4457112 (A.B.); +39-0862-433273 (M.M.). E-mail address: andrea.barbetta@uniroma1.it (A.B.); mara.massimi@univaq.it (M.M.).

† University of Rome "La Sapienza".

‡ University of L'Aquila.

10.1021/bm060533l CCC: $33.50
Published on Web 10/11/2006

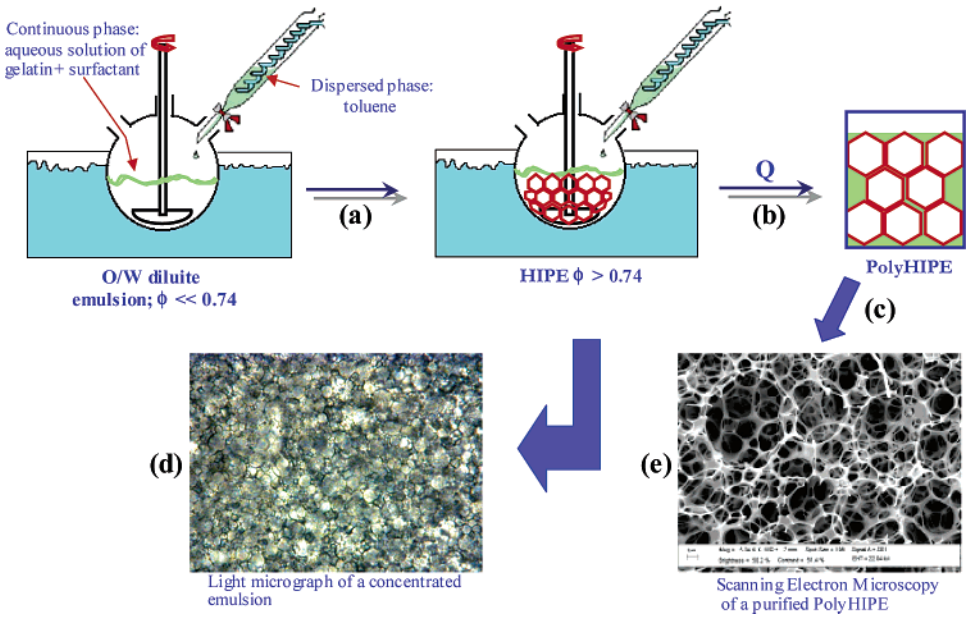

Figure 1. Schematic representation of HIPE synthesis (a) and polymerization of the external phase leading to a polyHIPE (b). In step c removal of the internal phase and purification from impurities (surfactant, MTGAse, additives) is performed by exchanging toluene with DMSO/ethanol and subsequent Soxhlet extraction with water/critical point drying. Figures shown in (d) and (e) refer to light and SEM micrographs of an HIPE and a polyHIPE, respectively.

compared. Primary rat hepatocytes were used as the main experimental cell system, because they represent a physiological model. We also used HepG2 cells, which are considered a suitable human model, as they are able to express most typical and differentiated human hepatocyte functions.[15]

Hepatocytes are widely used as a model to investigate physiopathological processes and offer a wide range of potential applications, including pharmacological and toxicological testing, cellular transplants, and bioartificial liver supports.[16] Experimental evidence has shown that the use of three-dimensional supports, such as the two-layer collagen gels,[17] woven capillary network,[18] nonwoven fabrics,[19] sponges, or foams,[20] may improve long-term hepatocyte functions. Although important progress has been made, there still remains a major challenge in designing an optimized 3D scaffold. Such a scaffold should provide an environment very similar to that found naturally in the liver lobule and should be able to guarantee a prolonged differentiated state of hepatocytes and, thus, enhanced liver-specific functions.

2. Experimental Section

2.1. Materials. Gelatin A3 (extracted from porcine skin and with a Bloom number equal to 300) and trinitrobenzenesulfonic acid (TBNS), 5% w/v solution in water, were supplied by Sigma-Aldrich. The surfactant Triton X-405 (70% w/v solution in water), methacrylic anhydride (MA), 2,2′-azoisobutyronitrile (AIBN), sodium chloride, dimethyl sulfoxide (DMSO), and toluene were purchased from Aldrich and used without further purification. Ca^{2+}-independent transglutaminase (MTGase) derived from the microorganism *Streptoverticillum* was kindly supplied by Chance and Hunt Food Ingredients, U.K. According to information from the supplier, the enzyme concentration in the preparation accounts for 1% w/w of the total material, the reminder being maltodextrin (99%).

2.2. PolyHIPE Synthesis. Gelatin A3 purification and the synthesis of its methacrylated derivative has been previously described in detail.[6,7] The procedure for the synthesis of gelatin A3 based polyHIPEs (cross-linked either by radical polymerization or enzymatically) is reported schematically in Figure 1a. The apparatus for the HIPEs preparation consists of a three-necked round-bottom flask fitted with a D-shaped paddle driven by an overhead stirrer and a condenser connected to a thermostat. The flask is partially submerged in a water bath maintained at 50 °C by a thermocouple, the temperature at which concentrated solutions of gelatin (typically, 20% w/v, based on the volume of the continuous phase) are fluid and processable into a HIPE. The organic phase (toluene) is added dropwise under stirring (300 rpm) from the thermostated (50 °C) condenser provided with a valve (Figure 1a). This guarantees that no heterogeneities arise locally within the emulsion as a consequence of the addition of drops of the dispersed phase at a lower temperature. A representative example of polyHIPE preparation is given: a solution of 0.5 g of gelatin (20% w/v) and 0.25 g of Triton X-405 (10% w/v, gross, with respect to the aqueous phase) were dissolved in 2.5 mL of PBS buffer, pH = 7.0. The solution was placed in the round-bottom flask, and the dispersed phase was added dropwise from the condenser under stirring. After completing the addition of toluene, MTGase dissolved in PBS, MTGase/gelatin = 1:1000 w/w was added to the emulsion and stirring was continued for 5 min to produce a homogeneous emulsion. An analogous procedure was followed in the case gelatin−methacrylate. After completing the addition of toluene, a radical initiator (AIBN, azobisisobutyrronitrile, 1% w/v with respect to the volume of the dispersed phase) dissolved in the minimum volume of toluene was added to the emulsion and stirring was continued for 10 min. The resulting HIPEs were transferred into a polyethylene bottle and placed in an oven set at 60 °C, in the case of gelatin−methacrylate, or at 50 °C, in the case of gelatin being cross-linked with MTGase, for 24 h. Foams with a nominal pore volume (PV = percentage of the volume of the oil discontinuous phase in the emulsion used to produce the matrix) of 85%, 90%, 92% were prepared using for the calculation of the volume of toluene to be used the formula reported below:

$$\mathrm{PV}\% = \frac{V_O}{V_O + V_A} \times 100 \qquad (1)$$

where V_O and V_A are the volume of the oil and aqueous phases, respectively.

Two different purification procedures were followed according to the cross-linking typology of the scaffolds. In the case of gelatin−poly(methacrylate), the solid monolith was soaked in DMSO, which

was changed regularly (typically three times a day) for 1 week. The solid foam was then Soxhlet extracted with water for 1 day and finally freeze-dried. In the case of enzymatically cross-linked gelatin, the solid foams were Soxhlet extracted with ethanol in order to displace both water and toluene and finally critical point dried with liquid CO_2.

In the following, gelatin methacrylated or gelatin cross-linked with MTGase scaffolds will be designated as GMAX or GMTGaseX, respectively, where X represents the pore volume calculated by means of eq 1. Solid foams obtained by employing additives in the emulsion formulation will be distinguished from the others by the presence in their coding names of the suffix *add* (e.g., GMAX*add*).

2.3. Determination of Pore and Interconnect Size Distributions. The internal structure, cavities (hereafter defined as voids), and pore throat size (hereafter defined as interconnects) of the polyHIPEs were studied using scanning electron microscopy (SEM) (LEO 1450VP) operating at 10 or 20 kV. Prior to observation, fractured samples were mounted on aluminum stubs using adhesive carbon disks to increase the conductivity. All samples were sputtered with a thin layer of gold (~10 nm) in argon atmosphere using a SEM coating unit 953, Agar Scientific, to ensure conductivity. The micrographs of all porous matrixes were used to determine the void and interconnect size of the polyHIPEs. In practice, several micrographs taken at a magnification that allowed us to view about 50 voids (or interconnects) at a time were collected from different areas chosen at random within the exposed surface of the specimen. Images of each sample were imported into the program SEMAfore, and the diameters of all the voids (D) and interconnects (d) (from a few to several hundreds) were measured and used to determine the number distributions of voids and interconnects as well as their average values ($\langle D \rangle$ and $\langle d \rangle$). To check reproducibility and to assign an error to $\langle D \rangle$ and $\langle d \rangle$, each polyHIPE was prepared in three different batches and diameter measurements were carried out on each of them. Errors are expressed as the standard deviations among the independent set of values.

2.4. Chemical Determination of Free Amine Groups in MTGase Gelatin Scaffolds. Freeze-dried gelatin gels cross-linked with MTGase (2−4 mg) were incubated in 2 mL of a solution of TNBS (0.01 M) in sodium hydrogen carbonate (pH 8.2, 4% w/v%) for 2 h at 40 °C. Then, hydrochloric acid (6 M, 3 mL) was added to the solution to hydrolyze the gelatin gels in 1.5 h at 60 °C. After cooling to room temperature, deionized water (5 mL) was added to the solution, and the absorbance at 345 nm was measured against a TNBS solution without gelatin, which had been treated in exactly the same way as the cross-linked gelatin samples. With the use of the adsorption coefficient of 2,4,6-trinitroaniline-derivatized (hydroxyl)lysine residues ($\epsilon = 14\,600$ L/(mol cm)),[21] the amount of free amine groups per 1000 amino acids was calculated, assuming a molecular weight for a gelatin chain of 1000 amino acids of 10^5 g/mol. The experiments were performed in triplicate.

2.5. Cell Culture. *2.5.1. Cell Isolation and Culture.* Male Wistar rats (150−180 g) kept on a standard ad libitum diet with free access to tap water were used, according to principles of laboratory animal care. Before surgery, the animals were anesthetized with an intraperitoneal injection of Farmotal (10 mg/100 g body weight; Farmitalia, Italy). Cells were isolated by perfusion of livers with collagenase (Sigma) according to the method of Moldeus et al.[22] Cell viability was assessed by Trypan-blue exclusion and was at least 90%. Highly differentiated HepG2 cells were obtained from the American Type Culture Collection (ATCC, Rockville, Maryland). Primary rat hepatocytes and HepG2 cells were suspended in Dulbecco's modified Eagle's medium/F12 (Gibco/BRL, MD) containing 10% fetal bovine serum, 2 mM L-glutamine, 100 μg/mL streptomycin and 100 U/mL penicillin (Sigma, St. Louis, MO), plated in 24-well culture plates containing the UV-sterilized biomaterials and incubated at 37 °C in a humidified atmosphere of 5% CO_2. The medium was changed 4 h after plating and subsequently every 24 h.

2.5.2. Cell-Loading Efficiency. For a general setting of our three-dimensional cell culture systems, primary hepatocytes at different initial densities ranging from 1.5 to 6.0 × 10^5 per well were seeded in 24-well culture plates containing the biomaterials of interest, carefully cut into 1 mm thick disks (Ø 12 mm). Four hours after seeding, unattached suspended hepatocytes were removed and carefully counted. Attached hepatocytes were estimated by subtracting this number from the initial seeding number, and the cell-loading efficiency was then calculated (percent of adherent cells in relation to the initial seeding density).[23] Statistical analysis was performed using Student's t-test. Differences with a p value <0.05 were considered significant.

2.5.3. Proliferation/Cytotoxicity Assay. The viability of the primary hepatocytes in the two different types of scaffolds after 24, 48, 72, and 96 h of culture was determined by means of MTS assay. Six small disks (Ø 0.5 cm, approximately 30 mm^3 wet volume) were randomly cut from each cell-seeded scaffold and placed in 96-well plates; 20 μL of Cell Titer 96 AQ_{ueous} One Reagent (Promega, Madison, WI) was then added to each well and left in contact with the cells for 3 h at 37 °C. MTS [3-(4,5-dimethylthiazol-2-yl)-5-(3-carboxymethoxyphenyl)-2-(4-sulfophenyl)-2H-tetrazolium] is bioreduced by metabolically active cells into a colored formazan product that is soluble in tissue culture medium.[24] For detection, the absorbance was measured at 490 nm. Values obtained in the absence of cells were considered as background. Statistical analysis was performed using Student's t-test. Differences with a p value <0.05 were considered significant.

2.5.4. Scanning and Confocal Laser Microscopy. The morphology of entrapped primary and HepG2 hepatocytes was examined by scanning electron microscopy (SEM). After fixation in 2.5% glutaraldeyde in pH 7.5 phosphate buffer, followed by postfixation in 1% osmium, cell-seeded scaffolds were dehydrated in a graded ethanol solution (from 30% to 100%). Samples were then critical point dried using liquid CO_2 and coated with 5 nm of vacuum-evaporated gold before examination under an XL 30 CP (Philips) scanning electron microscope.

For visualization of the junctional proteins E-cadherin and β-catenin, a standard protocol was followed[25] with minor modifications. Briefly, the entrapped cells were fixed in methanol at −20 °C for 15 min, washed with phosphate buffer saline (PBS), and incubated for 30 min in a blocking solution containing 1% bovine serum albumin and 5% normal goat serum, before being stained for 1 h with monoclonal antibodies to E-cadherin (1:80) or β-catenin (1:100) (Zymed Laboratories, CA). The specimens were then incubated with an antimouse AF455- or AF488-conjugate (1:200) (Molecular Probes Inc., Eugene, OR) and, following extensive washings, mounted on glass slides and coverslips, using an aqueous medium containing antifade to reduce the quenching of fluorescence. Similarly, some specimens of primary hepatocytes cultured under conventional two-dimensional conditions were treated for visualization of junctional proteins. All specimens were examined with a SARASTRO 2000 (Molecular Dynamics) confocal scanning laser microscope, equipped with an argon ion laser (25 mW), giving an excitation wavelength in the region of 458−514 nm, as the light source. Negative controls were performed by exposing specimens under similar conditions, while omitting the primary antibody.

3. Results and Discussion

3.1. Gelatin Scaffolds by Radical Polymerization. High internal phase emulsions, defined as having an internal droplet phase exceeding 74 vol % of the total volume of the emulsion, are highly viscous but liquid formulations. The high viscosity is a result of compressed droplets, which are polyhedral in shape but with relatively uniform droplet size distribution.[26] In Figure 1d a light micrograph illustrates the typical appearance of an HIPE. During the polymerization/cross-linking reaction of the continuous phase (Figure 1b) of HIPEs the structure of the emulsion acts as a template for the resulting porous interconnected polymer solid foam. The SEM micrograph of Figure 1e shows the characteristic morphology of the ensuing polyHIPE consisting of approximately spherical cavities (voids) interconnected by a plurality of window holes (interconnects).

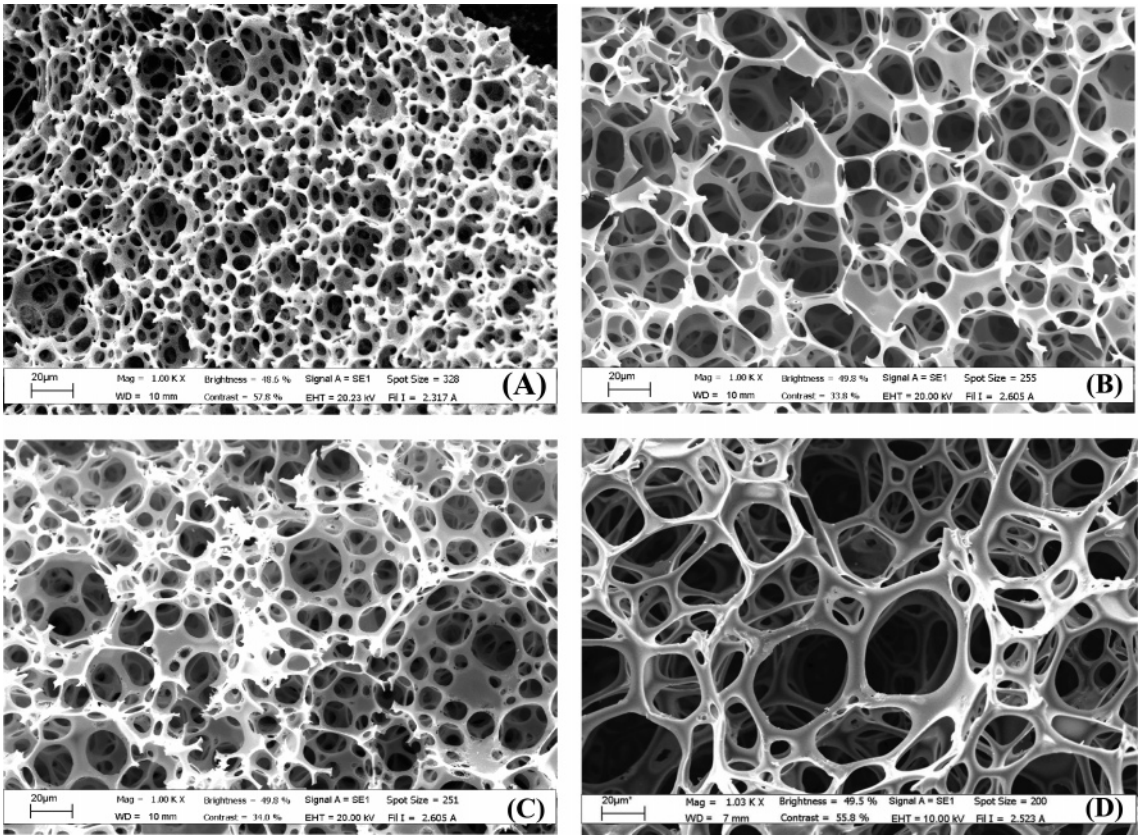

Figure 2. Scanning electron micrographs of GMA polyHIPE solid foams cross-linked by radical polymerization and characterized by two different pore volumes: (A and C) 90%; (B and D) 92%. Samples shown in parts C and D were obtained by using additives (0.01 M NaCl and 1% v/v DMSO).

GMA polyHIPEs were prepared and polymerized following the protocol described in the Experimental Section. Both the emulsions with a volume fraction of the dispersed phase of 90% and 92% were very stable at the temperature of synthesis (50 and 60 °C), and no phase separation occurred. It is well-known that droplet size decreases with increasing emulsion stability since the surface energy per unit area is lower. A decrease in emulsion droplet size leads to a decrease in polyHIPE void size since the solid foam is effectively a replica of the emulsion structure prior to gel formation. Already qualitatively, the analysis of SEM micrographs of GMA90 and GMA92 (Figure 2A and B) reveals that the void and interconnect diameters fall in the range of 5−20 and 5−10 μm, respectively. It is generally recognized[27] that pore size and total porosity of devices for tissue-engineering applications are critical to their ability to interact with cells and tissues following implantation, and interconnected pores greater than 100 μm are desirable. Thus, the matrixes presented in Figure 2, parts A and B, are unsuitable for their indented applications as the cells will not be able to migrate through the porous structure and give rise to true 3D colonization. In an effort to increase drastically the mean void and interconnect diameters, a controlled, partial destabilization of the precursor emulsion was induced. In a previous paper[6] we have demonstrated that by adding NaCl (0.01 M) to the aqueous phase and dimethyl sulfoxide (DMSO) (1% v/v) to the organic phase of an oil-in-water (O/W) emulsion, a considerable increase in both void and interconnect mean diameters can be obtained. The effect of NaCl is to reduce the solubility of Triton X-405 (salting out) in water at the HIPE processing temperature (50 °C) and to induce a reorganization of the packing geometry of the surfactant molecules at the O/W interface as a consequence of the dehydration of the hydrophilic part of the surfactant represented by polyoxyethylenic chains.[28] This causes both a depletion of the surfactant from the aqueous phase because of its increased partitioning in favor of the organic phase and a reduction of the surfactant excess at the O/W interface. The addition of small quantities of DMSO has the effect of diluting the surfactant interfacial layer as well. Furthermore, it enhances the molecular diffusion of toluene through the continuous phase from small droplets of the dispersed phase to larger ones, a phenomenon known as Ostwald ripening.[29] The combined effect of said additives is to increase the interfacial tension (γ). When the input of mechanical work (speed and duration of stirring) is kept constant, the effect of additives translates into the formation of larger voids. Such an approach was implemented with the parent emulsions of GMA90 and GMA92. The effect of said additives on the morphology of GMA polyHIPEs can be appreciated through the comparative analysis of the SEM micrographs reported in Figure 2, parts C and D, with those in parts A and B. A pronounced increase in both voids and interconnects sizes is evident.

Since the voids and interconnects are polydisperse in size, full characterization of the pore structure requires knowledge of the distributions of both voids and interconnects size. These can be evaluated by graphical measurements on SEM micrographs. This procedure involves an element of judgment, but by making a large number of measurements on micrographs taken from several regions of the sample (see the Experimental Section for details), useful comparative data could be obtained. Figure 3 shows number distributions $((N/N_t) \times 100$ for voids (a1 and b1) and interconnects (a2 and b2), where N_t is the total number of voids (interconnects) measured and N the number of voids (interconnects) within range. When the void size distributions of GMA90 (Figure 3a1) and GMA92 (Figure 3b1)

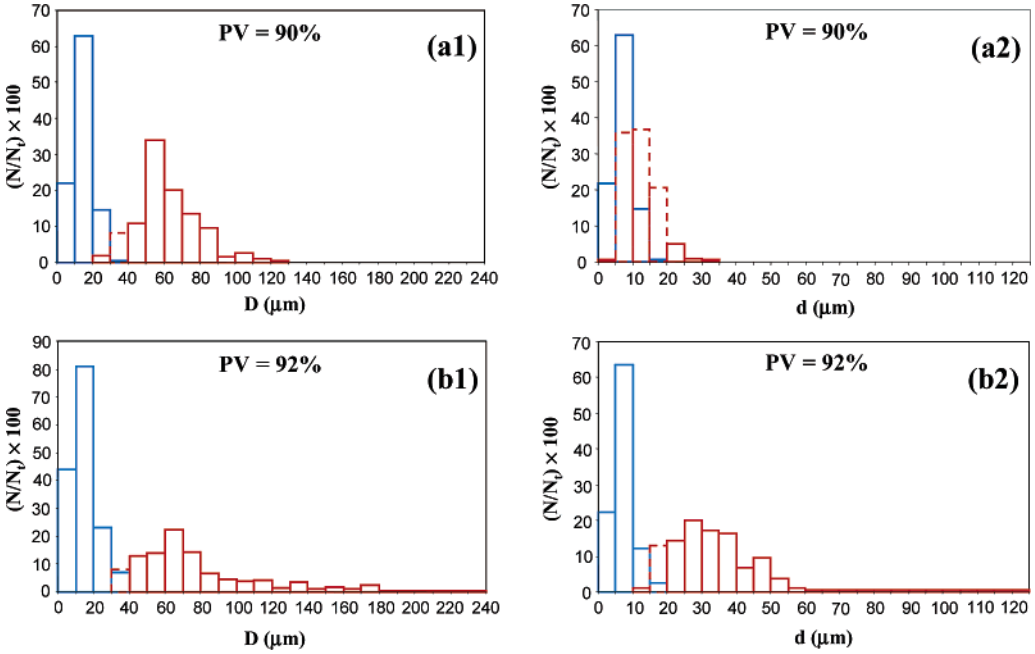

Figure 3. Number distributions of voids (a1, b1) and interconnects (a2, b2) size of GMA polyHIPE solid foams obtained without (blue line) and with (red line) additives (0.01 M NaCl and 1% v/v DMSO).

Table 1. Average Values of Voids and Interconnects of PolyHIPE Solid Foams and Number Percentage of Voids and Interconnects with Diameters Exceeding 50, 100, and 20 μm, respectively

sample	$\langle D \rangle$ μm	$\langle d \rangle$ μm	% D $\geq$ 50 μm	% D $\geq$ 100 μm	% d $\geq$ 20 μm
GMA90	14 ± 4	7 ± 2	0	0	0
GMA92	14 ± 4	8 ± 2	0	0	0
GMA90add	61 ± 5	12 ± 3	83 ± 4	6 ± 3	6.5 ± 2
GMA92add	84 ± 8	28 ± 6	85 ± 4	25 ± 5	78 ± 3
GMTGase85	19 ± 6	10 ± 3	0	0	0
GMTGase90	34 ± 6	12 ± 3	2 ± 1	0	0
GMTGase85add	26 ± 8	12 ± 6	2 ± 1	0	0
GMTGase90add	60 ± 10	18 ± 7	83 ± 6	34 ± 7	34 ± 5

solid foams obtained without (blue line) and with additives (red line) are compared, it can be seen that in the latter case there is a marked shift toward the large diameter side and a broadening of the distributions. Figure 3, parts a2 and b2, shows the corresponding number distributions of interconnect size. As with the void size, there is a general shift and broadening of the distributions even though less pronounced.

Table 1 summarizes results obtained from voids and interconnects diameters measurement on GMA polyHIPEs in terms of their average values ($\langle D \rangle$, $\langle d \rangle$) plus associated uncertainness and the percentages of voids with diameters exceeding either 50 or 100 μm and interconnects diameters $\geq$ 20 μm. As already pointed out qualitatively, the solid foams obtained without the employment of additives (GMA90 and GMA92) have no void with $D \geq 50$ μm and no interconnect with $d \geq 20$ μm. On the contrary, in the case of GMA90*add* and GMA92*add* solid foams, a high percentage of voids diameters exceeds 50 μm, with GMA92*add* displaying a significant contribution of voids with $D \geq 100$ μm and $d \geq 20$ μm. This is in agreement with the presence in both GMA92*add* void and interconnect diameters distributions (Figure 3, parts b1 and b2, red lines) of a long tail extending in the high-diameter range and with large values of $\langle D \rangle$ and $\langle d \rangle$ (Table 1). When the $\langle D \rangle$ values of couples of solid foams characterized by the same PV (90% or 92%) but differing by the absence or presence of additives in their HIPE formulations are compared, it can be seen that the percentage increment in $\langle D \rangle$ from GMA90 to GMA90*add* is about 350% and 500% from GMA92 to GMA92*add*. The same kind of analysis carried for $\langle d \rangle$ allows us to establish that a percentage increase of 80% and 280% was obtained for PV 90% and 92% solid foams, respectively.

The effect of destabilizing additives used in the present work on the HIPEs here examined is similar to that observed by other authors in the case of water-in-oil (W/ O) HIPEs.[2,3]

3.2. Gelatin Scaffolds by MTGase Cross-Linking. As a first experimental run, we tried to synthesize a foam characterized by a PV of 85% and with a concentration of gelatin A3 of 20% w/v dissolved in PBS buffer using a MTGase/gelatin ratio of 1:200 w/w. We discovered that the concentration and time of addition of MTGase to the emulsion is crucial. If the MTGase was present already in the aqueous phase of the HIPE from the very beginning of emulsion formation, cross-linking started during the addition of the organic phase. This prevented the formation of the HIPE. We were then forced to add MTGase dissolved in PBS at the end of emulsion formation in order to minimize the contact time with gelatin during the addition of the internal phase. Also the amount of MTGase added to the HIPE is important. If the MTGase/gelatin ratio exceeded 1:500, cross-linking started almost instantaneously, while still stirring the emulsion in order to disperse MTGase homogeneously within the entire volume of the HIPE. This led to a polyHIPE with a highly distorted morphology. We found that the scaffolds preserved the characteristic morphology of polyHIPEs when a MTGase/gelatin ratio of 1:1000 was used and stirring was stopped after 5 min after addition of the enzyme.

In Figure 4, parts a and b, SEM micrographs show the morphology of the solid foams characterized by PV 85% and 90% by following the preparation scheme outlined above. The skeletal framework of the solid foam is characterized by thinner walls with respect to GMA-type solid foams and, as a result, by weaker mechanical properties (from a qualitative point of view). We found also that the morphologies of the obtained GMTGase scaffolds were influenced by the method of purifica-

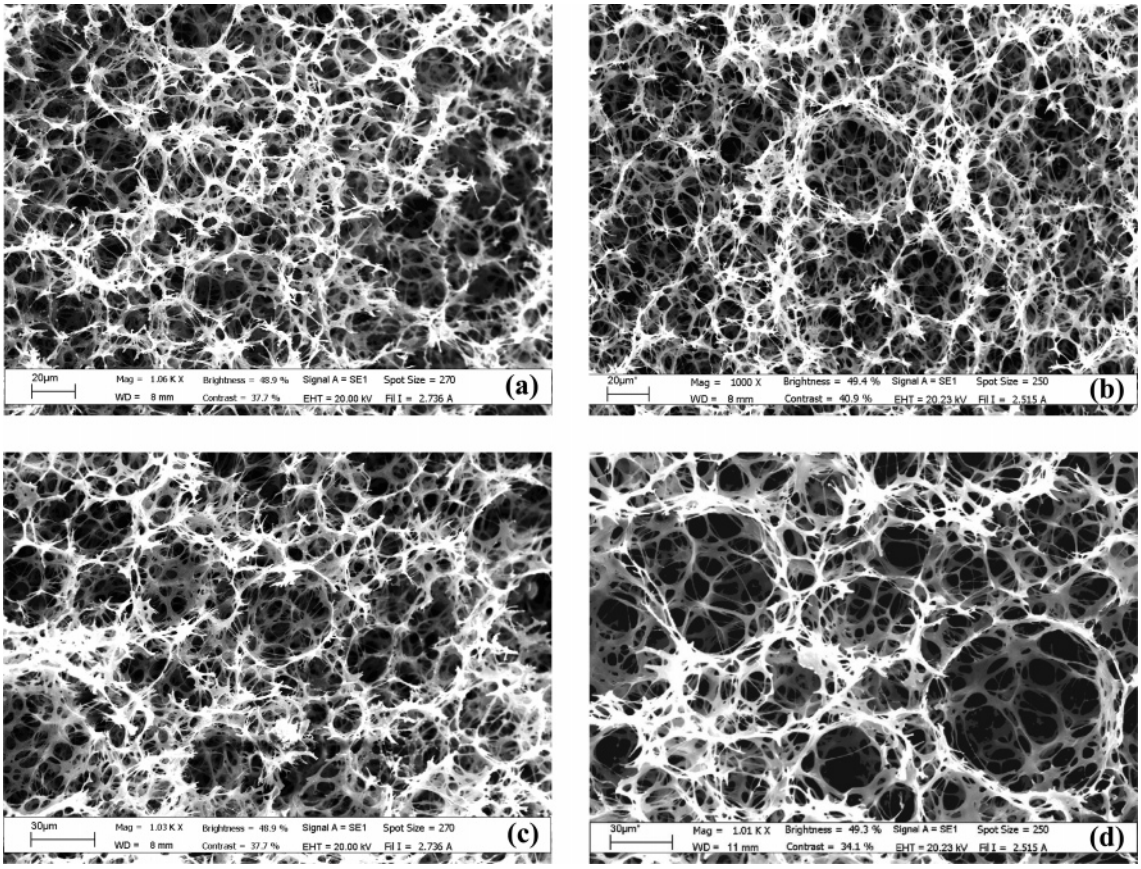

Figure 4. Scanning electron micrographs of gelatin A3 polyHIPE solid foams cross-linked with MTGase characterized by two different pore volumes: (a and c) 85%; (b and d) 90%. Samples shown in parts c and d were obtained by using additives (0.01 M NaCl and 1% v/v DMSO).

tion and drying. If freeze-drying was chosen as the drying procedure, the skeletal framework of the porous gel underwent a partial collapse. On the contrary, the drying procedure based on critical point drying by supercritical CO_2 has the advantage of leaving the porous texture quite intact. The average dimensions of voids and interconnects determined from analysis of SEM micrographs of GMTGase85 and GMTGase90 solid foams (Figure 4, parts a and b) are reported in Table 1. These values, again, are not adequate for the viable colonization of the scaffolds from seeded cells. The strategy devised for increasing both $\langle D \rangle$ and $\langle d \rangle$ in the case of GMA polyHIPEs was adopted also in the case of enzymatically cross-linked gelatin polyHIPEs. The same concentrations of NaCl and DMSO were employed in the emulsion formulation, and the outcome of such an approach can be observed in the micrographs reported in Figure 4, parts c and d. Again, the effect of additives resolves in a shift and broadening of the diameter distributions (Figure 5). Table 1 data shows that only GMTGase90*add* possesses a relevant percentage of voids and interconnects with diameters $\geq$ 100 and 20 μm, respectively.

The percentage increment in $\langle D \rangle$ and $\langle d \rangle$ was 36% and 18% for GMTGase85*add* and 76% and 33% for GMTGase90*add* with respect to GMTGase85 and GMTGase90, respectively.

We wondered what could be the origin of the fibrous-like appearance of the GMTGase polyHIPEs.

Some hypothesis are listed below.

3.2.1. Low Cross-Linking Density. From the amino acid composition of gelatin A3[13] it turns out that the theoretical cross-linking degree is dictated by the percentage of lysine and hydroxy lysine residues which bear primary amine groups. The carboxylic acid content in gelatin A3 is much higher than amine groups (80 vs 30 with respect to 1000 amino acids). Furthermore, the actual degree of cross-linking may be lower than this limit. The two-phases nature of the emulsion may have an influence on the activity of MTGase. Unpredictable small amounts of toluene are present in the aqueous phase due both to partitioning and molecular diffusion (Ostwald ripening).[30] The amount of organic solvents dissolved in the aqueous phase should be higher when DMSO is used as an additive because it will partition between the organic and aqueous phases and it will enhance both partitioning and diffusion of toluene through the continuous phase. Exposure of MTGase to small amounts of organic solvent, surfactant, and NaCl (which causes an increase in the ionic strength of the aqueous phase) may partially impair its activity giving rise to lower degrees of cross-linking.

This hypothesis was checked through the determination of the percentage of the residual free amino groups in substrates such as the "conventional gels" obtained by cross-linking with MTGase a gelatin solution at the same concentration of the aqueous phase of an HIPE (20% w/v), a polyHIPE obtained without using any additives, and a polyHIPE synthesized by employing additives. Such a comparison was based on a spectrophotometric method using trinitrobenzensulfonic acid[21] which allows the determination of the content of free amine groups.

If organic solvents and salt dissolved in the aqueous phase depress MTGase activity, a higher percentage of free amino groups should be detected in the polyHIPEs (without and/or with additives) with respect to the conventional gel.

As can be seen (Table 2), the percentage of residual free amine groups is higher in the polyHIPEs (independently from the presence of additives) than in the conventional gel. This means that the actual degree of cross-linking is lower in the

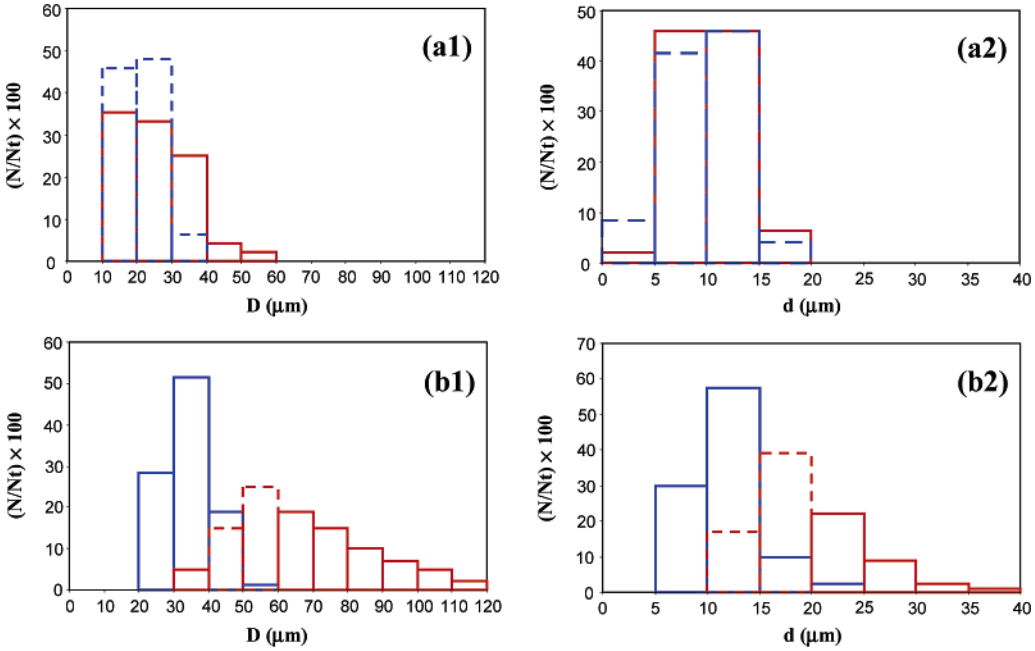

Figure 5. Number distributions of voids (a1, b1) and interconnects (a2, b2) size of gelatin A3 cross-linked with MTGase polyHIPE solid foams obtained without (blue line) and with (red line) additives (0.01 M NaCl and 1% v/v DMSO).

Table 2. Number of Amino Acids Residues Bearing Side Chain Amine Groups in Gelatin A3 and Percentages of Residual Free Amine Groups in Conventional Gel and in PolyHIPEs Cross-Linked with MTGase

no. of amino acids bearing NH_2 functionalities in gelatin A3[b]	residual % of amine groups[a]			
	conventional gel	PV %	GMTGase	GMTGase(add)
30	46	85	79	81
		90	80	78

[a] Determined by the method described in ref 21. [b] Number of free amine groups per 1000 amino acids.

polyHIPE than in the conventional gel. Thus, the two liquid phases of the emulsion do exert an influence on MTGase activity.

3.2.2. Nature of the Bridging Units. A structural feature influencing the different morphologies recorded by employing the two different modes of cross-linking resides on the different kind of bridges established among gelatin chains. In radical polymerization of the methacrylic moieties, a poly(methacrylate) chain develops among many interlinked gelatin chains. In enzymatic cross-linking an isopeptide junction joins two gelatin chains at a time, and as a consequence, the overall extent of networking is less efficient. On the other hand, Giraudier et al.[31] demonstrated that gelatin chains even when cross-linked by MTGase are able to undergo to some extent triple-helix formation on cooling at room temperature and after a maturation time, thus creating additional physical junction zones among gelatin chains (chemical−physical gel). This should aid in conferring to gelatin gels improved mechanical properties. Nevertheless, in the present case the very low density of chemical cross-linking and kind of chemical junctions are on the overall at the basis of the relatively poor mechanical properties of GMTGase polyHIPEs as compared to those of the GMA type.

This explains why GMTGase polyHIPEs when exposed to high vacuum, during freeze-drying, undergo a partial collapse of the porous structure.

3.3. Cell Studies. When hepatocytes are removed from the architectural liver, formation of cell aggregates in the hydrogel scaffold is a requisite for enhancing liver-specific functions. Thus, in liver tissue engineering, the scaffolds sustaining the self-assembling of hepatocytes into aggregates must have appropriate dimension of pores in order to host such aggregates. As a consequence, in the context of the present study, the most promising candidates of the two differently cross-linked types of polyHIPEs that were tested for three-dimensional cultures of primary rat and HepG2 hepatocytes are GMA92*add* and GMTGase90*add* (Table 1).

We first tried to optimize the system by selecting the appropriate number of primary hepatocytes to be seeded in each well. As expected, the number of cells that could be entrapped in the matrixes increased with the seeding density, reaching a maximum value that depended on the affinity of the material for that kind of cell. A maximum of 3.9×10^5 cells entrapped per well was found in GMTGase scaffolds, while the number of cells attached was appreciably lower in GMA92*add* scaffold (3.2×10^5). A density of 3.0×10^5 per well (24-well plate) was then chosen for all the experiments with primary hepatocytes. By calculating the cell-loading efficiency, we found that enzymatic reticulation was helpful for initial cell attachment (Figure 6). Initial cell density was found to be less critical for HepG2 cells (data not shown); however, a seeding density of 1.5×10^5 per well was considered appropriate for these proliferating cells.

From a morphological point of view, the scaffold more suitable for hepatocyte colonization should be GMA92*add* since, as is evident from data reported in Table 1, it is the one characterized by larger voids and interconnects in comparison to GMTGase90*add*. Nevertheless, cell-loading efficiency data, Figure 6, are higher for the second type of scaffold, indicating that not only are the differences in porosity between the two types of scaffolds not relevant but that hepatocytes seem to display a better affinity for the GMTGase90*add* matrix.

The viability of the primary hepatocytes in the scaffolds and, indirectly, the cytotoxicity of polymers were analyzed using MTS, a compound that can only be metabolized by healthy cells.

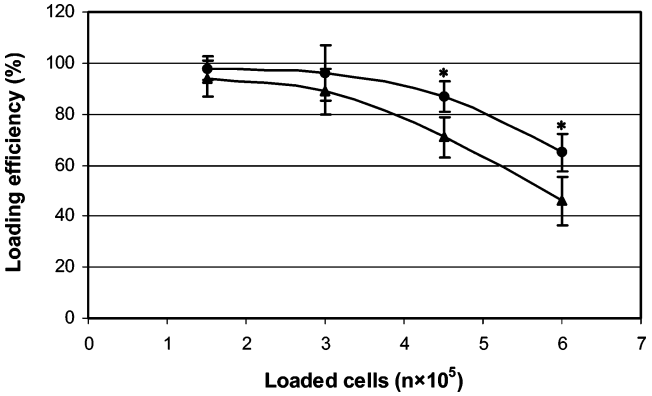

Figure 6. Cell-loading efficiency of primary rat hepatocytes within GMA92*add* (▲) and GMTGase90*add* (●) scaffolds. Data are expressed as the mean value ± standard deviation of at least three different experiments done in triplicate. Quantitative parameters were compared using the Student's *t*-test. ∗ Significant with respect to GMA92*add*, $P < 0.05$.

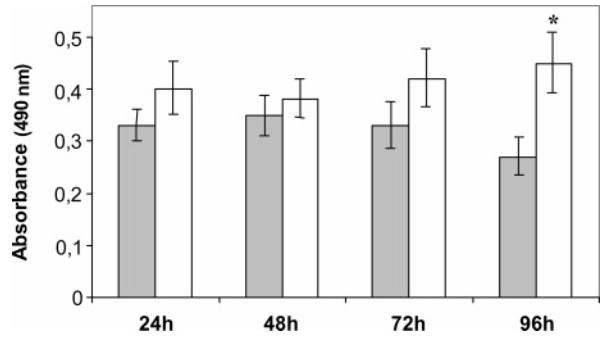

Figure 7. Cell viability assay (MTS) on primary hepatocytes cultured on GMA92*add* (grey bars) and GMTGase90*add* (white bars) scaffolds. Data are expressed as the mean 490 nm absorbance ± standard deviation of at least three different experiments done in quadruplicate. Quantitative parameters were compared using the Student's *t*-test. ∗ Significant with respect to GMA92*add*, $P < 0.05$.

Cell viability was satisfactory during the first 72 h of culture, without significant differences, on both GMA92*add* and GMTGase90*add* scaffolds. At 96 h, the absorbance, and thus the number of viable cells, was significantly higher for the GMTGase90*add* scaffold (Figure 7). These results were comparable to that observed in two-dimensional cultures until 48 h. However, at longer time the number of viable hepatocytes decreased of about 30% under conventional culture conditions, suggesting that our matrixes are more suitable for preserving cell integrity and viability for long-term maintenance.

The ultrastructural analysis, performed by SEM, showed that both primary hepatocytes (Figure 8, parts a and c) and HepG2 cells (Figure 10, parts a and d) adhered on both the polymers tested, with a homogeneous colonization of the scaffolds. This was particularly consistent with scaffolds obtained with radical polymerization (GMA92*add*), which are characterized by a greater stability and a better defined morphology. Nevertheless, on the GMTGase90*add* scaffold, cell aggregates were larger and better organized in the three-dimensional space than those on the GMA92*add* scaffold. In addition, both GMTGase90*add*-seeded hepatocytes and HepG2 cells displayed an improved morphology and a better quality of their cell surfaces, with abundant and regular microvilli. They also appear more closely connected, suggesting the presence of better organized cell junctions (Figure 8, parts b and d; Figure 10, parts a and d). On the other hand, the GMTGase90*add* scaffold resulted in more fragility and less resistance in longer-term cultures.

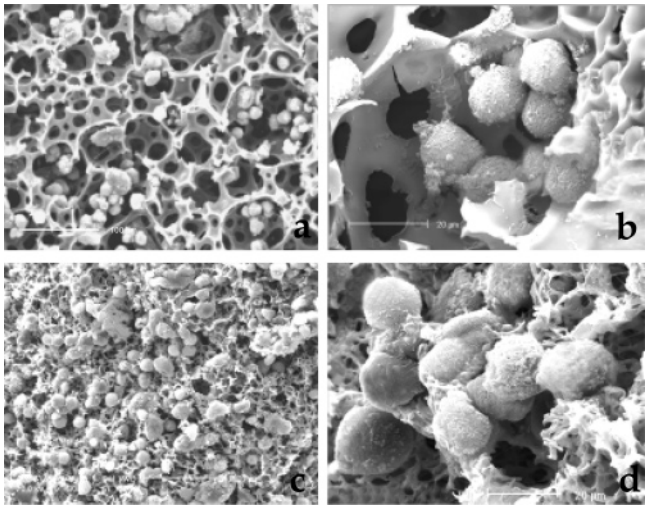

Figure 8. Low (a, c) and high (b, d) magnification scanning electron micrographs of primary rat hepatocytes cultured for 72 h on GMA92*add* (a, b) or GMTGase90*add* scaffolds (c, d).

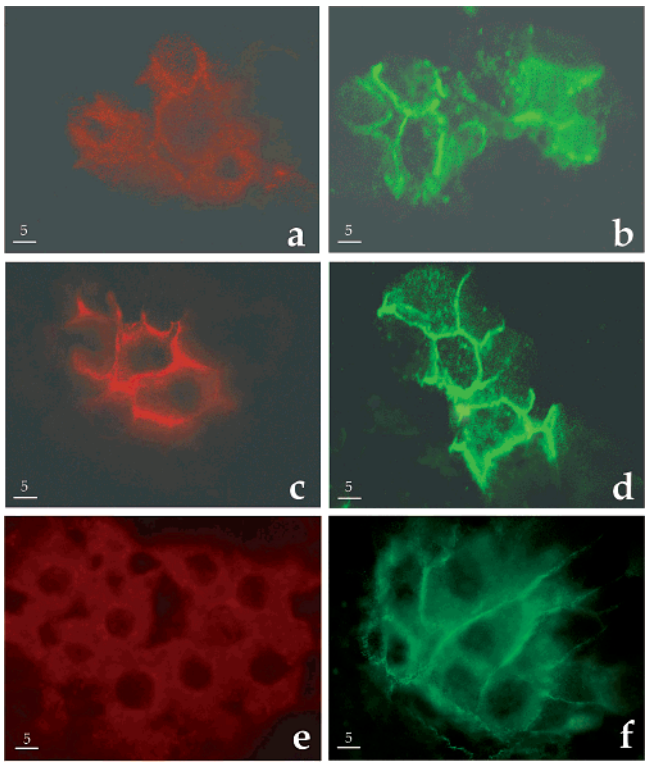

Figure 9. Confocal laser microscopy of the junctional proteins E-cadherin (a, c, e) and β-catenin (b, d, f) in primary rat hepatocytes cultured for 72 h on GMA92*add* (a, b) or GMTGase90*add* scaffolds (c, d) or in two-dimensional cultures (e, f).

The expression of a differentiated phenotype is strictly dependent on cell−cell adhesion, which is highly critical for all epithelial cells, including hepatocytes. An impaired expression of cell-junctional molecules, and of E-cadherin and β-catenin in particular, is often correlated with cell dedifferentiation and/or transformation.[32]

A certain degree of dedifferentiation is always observed in primary hepatocytes under standard conventional monolayer cultures, and it has sometimes been associated with the lack of appropriate contacts between neighboring cells.[33] The reestablishment of optimal cell−cell interactions is thus indicative of a functional cell recovery. By means of immunofluorescence experiments and confocal laser microscopy, we verified the

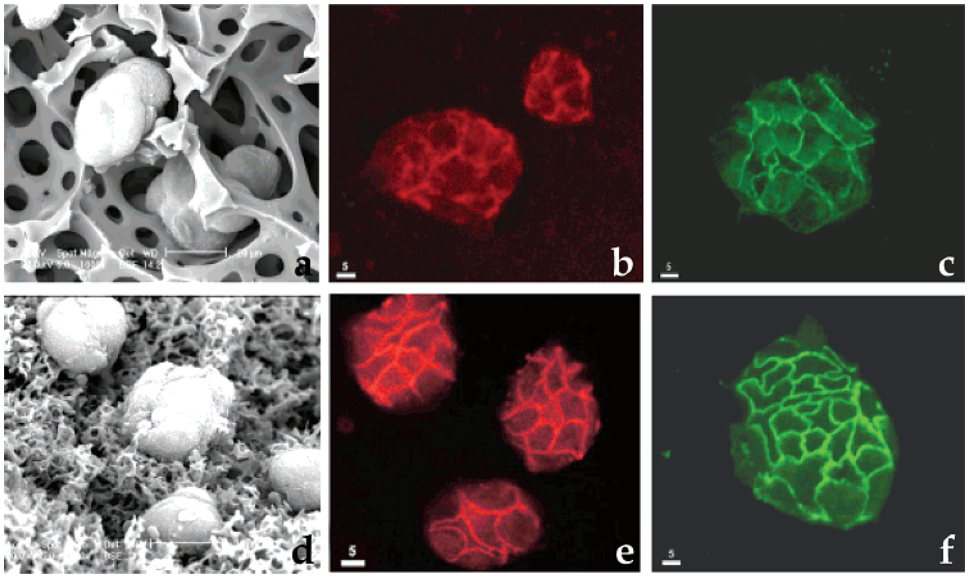

Figure 10. Scanning (a, d) and confocal laser microscopy (b, c, e, f) of HepG2 cells cultured for 72 h on GMA92*add* (a, b, c) or GMTGase90*add* scaffolds (d, e, f). Immunofluorescence of the junctional protein E-cadherin (b, e) and β-catenin (c, f).

correct expression of these two key adhesion proteins in normal and proliferating hepatocytes, cultured on both the GMA92*add* and GMTGase90*add* three-dimensional scaffolds. In the case of primary hepatocytes, while the GMTGase90*add* scaffold showed a good expression of both E-cadherin and β-catenin (Figure 9, parts c and d), only β-catenin was appreciably expressed in GMA92*add* matrix (Figure 9b). In addition, in GMA92*add* scaffold (Figure 9, parts a and b) the positivity was lower and not confined to the cell membrane but also scattered in the cytoplasm, suggesting a less adequate localization. In standard two-dimensional conditions, both proteins appeared reduced in expression and delocalized from plasma membrane (Figure 9, parts e and f), strongly highlighting the better influence of enzymatic reticulation on the localization and expression of these adhesion molecules.

The images concerning immunolocalization experiments with HepG2 cells also agree with the primary hepatocyte results (Figure 10b,c,e,f). Also in this case, both scaffolds supported the expression of E-cadherin (Figure 10, parts b and e) and β-catenin (Figure 10, parts c and f); however, in cells seeded in GMTGase90*add* scaffold the labeling was stronger and present mostly at the level of the cell membranes, indicating a more correct localization (Figure 10, parts e and f). These findings, when compared with data reported in the literature concerning E-cadherin and β-catenin visualization in conventional bidimensional culture,[25,34] still indicate the positive effect of the three-dimensional architecture on the expression of a differentiated phenotype. In addition, in these proliferating cells (HepG2), the fluorescence labeling also put into evidence the larger size of the cell aggregates present on the enzymatic cross-linked biomaterial. These results were evident after 72 h of culture but were also detectable at shorter intervals (data not shown).

Taken together, our immunofluorescence studies show that in the GMTGase90*add* scaffold, E-cadherin and β-catenin both localize on the plasma membranes of normal or growing hepatocytes, and the scattered positivity distributed on whole cells completely disappears, indicating total insertion of the adherens complexes at the level of the cell contacts. This is in accordance with the superior organization of the cell aggregates observed by SEM analysis, and it seems to point to an enhanced biocompatibility of these materials.

4. Conclusion

The work presented in this paper compares the influence of two different cross-linking procedures on the morphology of emulsion-templated gelatin solid foams. Radical polymerization allows the production of foams characterized by larger voids and interconnects and with a better wall texture than those characterizing foams cross-linked with MTGase. The latter type of solid foams on the contrary seems to provide a more friendly environment for hepatocytes, presumably thanks to the absence of any foreign chemical functionalities, thus allowing us to exploit fully the biocompatible nature of gelatin. In this matrix, hepatocytes show not only good levels of vitality but also larger cell aggregates and were able to establish satisfactory cell−cell contacts, as indicated by the high and correct expression of specific molecules, i.e., the junctional proteins E-cadherin and β-catenin, known to be extremely important for maintenance of the differentiated phenotype and, in turn, for hepatocyte functionality.[32]

Efforts are currently being directed to envisage different foaming procedures and zero-bridges cross-linking methods able to give rise to more robust foams and possessing larger voids and interconnects. Such a cross-linking method under investigation is based on the use of the system *N*,*N*-(3-(dimethylamino)-propyl-*N*-ethyl carbodiimide (EDC) and *N*-hydroxysulfosuccinimide (NHSS).

Acknowledgment. The authors thank Mr. Robert Cant of Chance and Hunt Food Ingredients, U.K. for the kind supply of microbial transglutaminase and the University of Rome (Ateneo Funds) and Consorzio Interuniversitario Biotecnologie (CIB) for funding this research. We also thank Dr. D. Ferro of the Department of Chemistry of the University of Rome and The Microscopy Core Facilities of University of L'Aquila for the invaluable help with the confocal and scanning electron microscopy.

References and Notes

(1) Akay, G.; Birch, M. A.; Bokhari, M. A. *Biomaterials* **2004**, *25*, 3991−4000.
(2) Hayman, M. W.; Smith, K. H.; Cameron, N. R.; Przyborski, S. A. *Biochem. Biophys. Res. Commun.* **2004**, *314*, 483−488.

(3) Hayman, M. W.; Smith, K. H.; Cameron, N. R.; Przyborski, S. A. *J. Biochem. Biophys. Methods* **2005**, *62*, 231−240.
(4) Busby, W.; Cameron, N. R.; Jahoda, J. A. B. *Biomacromolecules* **2001**, *2*, 154−164.
(5) Busby, W.; Cameron, N. R.; Jahoda, J. A. B. *Polym. Int.* **2002**, *51*, 871−881.
(6) Barbetta, A.; Dentini, M.; Zannoni, E. M.; De Stefano, M. E. *Langmuir* **2005**, *21*, 12333−12341.
(7) Barbetta, A.; Dentini, M.; De Vecchis, M. S.; Filippini, P.; Formisano, G.; Caiazza, S. *Adv. Funct. Mater.* **2005**, *15*, 118−124.
(8) (a) Ferreira, L.; Gil, M. H.; Cabrita, A. M. S.; Dordick, J. S. *Biomaterials* **2005**, *26*, 4707−4716. (b) Huang, X.; Nayak, B. R.; Lowe, T. L. *J. Polym. Sci., Part A: Polym. Chem.* **2004**, *42*, 5054−5066. (c) Na, K.; Shin, D.; Yun, K.; Park, K.-H.; Lee, K. C. *Biotechnol. Lett.* **2003**, *25*, 381−385. (d) Kim, S.; Chae, S. Y.; Na, K.; Kim, S. W.; Bae, Y. H. *Biomaterials* **2003**, *24*, 4843−51. (e) Na, K.; Shin, D.; Yun, K.; Park, K.-H.; Lee, K. C. *Biotechnol. Lett.* **2003**, *25*, 381−5. (f) Kim, H.-W.; Song, J.-H.; Kim, H.-E. *Adv. Funct. Mater.* **2005**, *15*, 1988−1994. (g) Chang, C.-H.; Kuo, T.-F.; Lin, C.-C.; Chou, C.-H.; Chen, K.-H.; Lin, F.-H.; Liu, H.-C. *Biomaterials* **2006**, *27*, 1876−1888. (h) Young, S.; Wong, M.; Tabata, Y.; Mikos, A. G. *J. Controlled Release* **2005**, *109*, 256−274. (i) Huang, Y.; Onyeri, S.; Mbonda, S.; Moshfeghian, A.; Madihally, S. V. *Biomaterials* **2005**, *26*, 7616−7627. (j) Yang, S.-H.; Chen, P.-Q.; Chen, Y.-F.; Lin, F.-H. *J. Biomed. Mater. Res.* **2005**, *74B*, 488−494.
(9) (a) Schorsch, C.; Carrie, H.; Clark, A. H.; Norton, I. T. *Int. Dairy J.* **2000**, *10*, 519−528. (b) Motoki, M.; Seguro, K. *Trends Food Sci. Technol.* **1998**, *9*, 204−210.
(10) Fuchsbauer, H. L.; Gerber, U.; Engelmann, J.; Seeger, T.; Sinks, C.; Hecht, T. *Biomaterials* **1996**, *17*, 1481−1488.
(11) (a) Balakrishnan, B.; Jayakrishnan, A. *Biomaterials* **2005**, *26*, 3941−3951. (b) Crescenzi, V.; Francescangeli, A.; Taglienti, A. *Biomacromolecules* **2002**, *3*, 1384−1391. (c) Chen, T.; Small, D. A.; McDermott, M. K.; Bentley, W. E.; Payne, G. F. *Biomacromolecules* **2003**, *4*, 1558−1563.
(12) (a) Embree, H. D.; Brown, E. M.; Taylor, M. M.; Payne, G. F. *Biomaterials* **2003**, *24*, 2831−2841. (b) Mi, F.-L. *Biomacromolecules* **2005**, *6*, 975−987.
(13) San, Y.; Giraudier, O.; Garde, V. L. *Biopolymers* **2005**, *77*, 257−263.
(14) Ray-Neng, C.; Hsiu-O, H.; Ming-Thau, S. *Biomaterials* **2005**, *26*, 4229−4235.
(15) (a) Kelly, J. H.; Darlington, G. J. *In Vitro Cell. Dev. Biol.* **1989**, *25*, 217−222. (b) Hongo, T.; Kajikawa, M.; Ishida, S.; Ozawa, S.; Ohno, Y.; Sawada, J.; Umezawa, A.; Ishikawa, Y.; Kobayashi, T.; Honda, H. *J. Biosci. Bioeng.* **2005**, *99*, 237−44.
(16) (a) McLaughlin, B. E.; Tosone, C. M.; Custer, L. M.; Mullon, C. *Ann. N.Y. Acad. Sci.* **1999**, *875*, 310−325. (b) Katherine, M. K.; Vacanti, J. P. *Transplant Immunol.* **2004**, *12*, 303−10. (c) Hongo, T.; Kajikawa, M.; Ishida, S.; Ozawa, S.; Ohno, Y.; Sawada, J.; Umezawa, A.; Ishikawa, Y.; Kobayashi, T.; Honda, H. *J. Biosci. Bioeng.* **2005**, *99*, 237−44. (d) Vanhaecke, T.; Rogiers, V. *Methods Mol. Biol.* **2006**, *320*, 209−27.
(17) (a) Dunn, J. C. Y.; Tomkins, R. G.; Yarmush, M. L. *Biotechnol. Prog.* **1991**, *7*, 237−242. (b) Wang, Y. J.; Liu, H. L.; Guo, H. T.; Wen, H. W.; Liu, J. *World J. Gastroenterol.* **2004**, *10*, 699−702.
(18) Gerlach, J.; Schnoy, N.; Smith, M. D.; Neuhaus, P. *Artif. Organs* **1994**, *18*, 1−5.
(19) Catalano, G.; De Bartolo, L.; Vico, V.; Ambrosio, L. *Biomaterials* **2001**, *22*, 659−65.
(20) (a) Kaufmann, P. M.; Heimrath, S.; Kim, B. S.; Mooney, D. J. *Cell Transplant.* **1997**, *6*, 463−468. (b) Glicklis, R.; Shapiro, L.; Agbaria, R.; Merchuk, S. C. *Biotechnol. Bioeng.* **2000**, *67*, 344−353. (c) Li, J.; Pan, J.; Zhang, L.; Yu, Y. *Biomaterials* **2003**, *24*, 2317−22.
(21) Kuijpers, A. J.; Engbers, G. H. M.; Feijen, J.; De Smedt, S. C.; Meyvis, T. K. L.; Demeester, J.; Krijgsveld, J.; Zaat, S. A. J.; Dankert, J. *Macromolecules* **1999**, *32*, 3325−3333.
(22) Moldeus, P.; Holdberg, J.; Orrenius, S. *Methods Enzymol.* **1978**, *52C*, 60−71.
(23) Park T. G. *J. Biomed. Mater. Res.* **2002**, *59*, 127−35.
(24) Riss, T. L.; Moravec, R. A. *Mol. Biol. Cell.***1992**, (Suppl. 3), 184a.
(25) Ara, C.; Conti Devirgiliis, L.; Massimi, M. *Cell Commun. Adhes.* **2004**, *11*, 13−23.
(26) (a) Lissant, K. J. *J. Colloid Interface Sci.* **1966**, *22*, 462−468. (b) Lissant, K. J. *J. Colloid Interface Sci.* **1973**, *42*, 201−208. (c) Lissant, K. J.; Peace, B. W.; Wu, S. H.; Mayhan, K. G. *J. Colloid Interface Sci.* **1974**, *47*, 416−423. (d) Cameron, N. R.; Sherrington, D. C. *Adv. Polym Sci.* **1996**, *126*, 163−214. (e) Cameron, N. R. *Polymer* **2005**, *46*, 1439−1449.
(27) (a) Agrawal, C. M.; Ray, R. B. *J. Biomed. Mater. Res.* **2001**, *55*, 141−150. (b) Hollinger, J. O.; Leong, K. *Biomaterials* **1996**, *17*, 187−194. (c) Hu, Y. H.; Grainger, D. W.; Hollinger, J. O. *J. Biomed. Mater. Res.* **2002**, *59*, 563−572.
(28) (a) Schott, H. *J. Colloid Interface Sci.* **1998**, *205*, 496−502. (b) Goel, S. K. *J. Colloid Interface Sci.* **1999**, *212*, 604−606.
(29) Kabalnov, A. S.; Pertsov, A. V.; Shchukin, E. D. *J. Colloid Interface Sci.* **1987**, *118*, 590−597.
(30) Barbetta, A.; Cameron, N. R. *Macromolecules* **2004**, *37*, 3188−3201, 3202−3213.
(31) Giraudier, S.; Hellio, D.; Djabourov, M.; Larreta-Garde, V. *Biomacromolecules* **2004**, *5*, 1662−1666.
(32) (a) Kirkpatrick, C.; Peifer, M. *Curr. Opin. Genet. Dev.* **1995**, *5*, 56−65. (b) Ihara, A.; Koizumi, H.; Hashizume, R.; Uchikoshi, T. *Hepatology* **1996**, *23*, 1441−1447. (c) Knudsen, K. A.; Frankowski, C.; Johnson, K. R.; Wheelock, M. J. *J. Cell Biochem.* **1998**, (Suppl. 30/31), 168−176. (d) Gumbiner, B. M. *J. Cell Biol.* **2000**, *148*, 399−403. (e) Wei, Y.; Fabre, M.; Branchereau, S.; Gauthier, F.; Perilongo, G.; Buendia, M. A. *Oncogene* **2000**, *19*, 498−504.
(33) Yuasa, C.; Tomita, Y.; Sono, M.; Ishimura, K.; Ichihara, A. *J. Cell. Physiol.* **1993**, *156*, 522−530.
(34) Lin, C. Y.; Lin, C. J.; Chen, K. H.; Wu, J. C.; Huang, S. H.; Wang, S. M. *FEBS Lett.* **2006**, *580*, 3042−350.

BM060533L